Cu-Co dual-atom catalysts supported on hierarchical USY zeolites for the efficient cross-dehydrogenative C(sp^2)–N coupling reaction

Tianxiang Chen,[a,b,§] Wenhua Yu,[c,§] Ching Kit Tommy Wun,[a] Tai-Sing Wu,[d] Mingzi Sun,[a] Sarah J. Day,[e] Zehao Li,[f] Bo Yuan,[g] Yong Wang,[a] Mingjie Li,[h] Zi Wang,[i] Yung-Kang Peng,[g] Wing-yiu Yu,[a] Kwok-yin Wong,[a] Bolong Huang,[a,b,*] Taoyuan Liang,[c,*] Tsz Woon Benedict Lo[a,b,h,*]

a: The Hong Kong Polytechnic University Shenzhen Research Institute, The Hong Kong Polytechnic University, Shenzhen, 518057, China

b: State Key Laboratory of Chemical Biology and Drug Discovery, Department of Applied Biology and Chemical Technology, The Hong Kong Polytechnic University, Hong Kong, China

c: Guangxi Key Laboratory of Electrochemical Energy Materials, School of Chemistry and Chemical Engineering, Guangxi University, Nanning, Guangxi 530004, China

d: National Synchrotron Radiation Research Center, 101 Hsien-Ann Road, Hsinchu, 30076, Taiwan

e: Diamond Light Source Ltd., Harwell Science and Innovation Campus, Didcot, Oxfordshire, Harwell Campus, Oxford, OX11 0DE, United Kingdom

f: School of Chemistry and Chemical Engineering, Anyang Normal University, Anyang, 455000, China

g: Department of Chemistry, The City University of Hong Kong, Hong Kong, China

h: Department of Applied Physics, The Hong Kong Polytechnic University, Hong Kong, China

i: Department of Chemistry, University of Manchester, Manchester M13 9PL, United Kingdom

§ These authors contribute equally to this work.

* *Corresponding authors.*

E-mail addresses: bhuang@polyu.edu.hk (B. Huang), taoyuanliang@gxu.edu.cn (T. Liang), benedict.tw.lo@polyu.edu.hk (T. W. B. Lo)

KEYWORDS. Dual-atom Cu-M catalysts, hierarchical zeolite supports, co-adsorption-co-activation, cross dehydrogenative coupling, solid atomic catalysts.

ABSTRACT: Cross-coupling reaction *via* the dehydrogenative route over heterogeneous solid atomic catalysts offers practical solutions toward economical and sustainable elaboration of simple organic substrates. Current utilization of this technology is, however, hampered by limited molecular definition of many solid catalysts. Here, we report the development of Cu-M dual-atom catalysts (where M = Co, Ni, Cu, and Zn) supported on hierarchical USY zeolite to mediate the efficient dehydrogenative cross-coupling of unprotected phenols with amine partners. Over 80% isolated yields have been attained over Cu-Co-USY, which shows much superior reactivity when compared with our Cu_1 and other Cu-M analogs. This amination reaction has hence involved simple and non-forceful reaction condition requirements. The superior reactivity can be attributed to (1) the specifically designed bimetallic Cu-Co active sites within the micropore for 'co-adsorption-co-activation' of the reaction substrates, and (2) the facile intracrystalline (meso/micropore) diffusion of the heterocyclic organic substrates. This study offers critical insights into the engineering of next-generation solid atomic catalysts where complex reaction steps.

INTRODUCTION

With the global economic boom and population growth, sustainable provision of fine, optoelectronics, and pharmaceutical chemicals has become one of the most important issues in modern society, which often involves the use of catalytic processes. Heterogeneous solid atomic catalysts – with well-defined active site architecture – have attracted immense attention in recent years for sustainable organic transformations. The versatility of solid atomic catalysts has driven a wide range of applications in organic transformation processes, such as direct arylations, hydrosilylation,[1] hydroboration,[2] and C–C/C–X cross-

coupling reactions.[3-6] Particularly, a series of single-atom catalysts (a sub-class of solid atomic catalysts) have been reported over various support materials, including zeolites,[7] metal-organic frameworks,[8-11] graphitic carbon nitride,[12] metal oxides,[13] *etc.*[14-18], for cross-coupling reactions. Seminal work by de Vos *et al.* reported the development of molecular Pd within zeolites to achieve high selectivity toward *para*-biaryl compounds by C(sp^2)–H activation *via* zeolitic steric confinement.[7] In essence, solid atomic catalysts can bring heterogeneous catalysts toward the molecular frontier, as they can not only render high potential in matching the performance of the *state-of-the-art* homogeneous organometallic catalysts but also allow facile separation of catalysts from the reaction mixture for process intensification.[19-21] However, the catalytic capability of most solid atomic catalysts for reactions that involve multiple reaction steps is still not yet satisfactory and broader applications remain generally unexplored. It has been attributed to the generally lower molecular definition of the active site architecture and the less mature tunability in steric and electronic properties to achieve further complex functional derivatization.[22]

For cross-coupling reactions where multiple complex steps are involved, neighboring metal sites (*e.g.*, in dual-atom catalysts) are shown to be effective in promoting catalytic efficacy through optimizing the synergy by co-adsorption and subsequent co-activation of different reaction substrates by separate metal sites, which could further influence the adsorption structures to break the scaling relationship limits.[23-25] Pairing of metals could further alter the electronic states, and break the limitations of symmetric charge distribution by polarization, which would influence the catalytic characteristics in a manner that is impossible with most analogous single-atom catalysts. Porous materials like zeolites, metal- and covalent-organic frameworks, and polyoxometalates can be utilized as ideal domains for the engineering of precise dual-atomic, or even multi-atomic catalytic species.[26] By enabling the exploitation of confinement-controlled chemistry within the quasi-isolated pores of molecular dimension, simultaneous activation of coupling partners and stabilization of the reactive intermediates can be favored.[27-28]

Here, we demonstrate that Cu-Co dual-atom active sites supported on hierarchical USY zeolites can allow the efficient cross-dehydrogenative coupling (CDC) of unprotected phenols with phenothiazines to form aminated phenols. By fine-tuning the constituent components of Cu: M (among M = Co, Ni, Cu, and Zn), the optimal reactivity of the catalysts has been achieved at Cu-Co supported on USY zeolite. Notably, its conversion is nearly two-fold magnitude greater than the single-atom Cu_1 counterpart, showing exceptional reactivity with simple and non-forceful reaction condition requirements, namely, room temperature, air (or O_2), methanol as solvent, and additive-free. The catalysts also show high catalytic stability from our recycling experiment with no observed metal leaching. A high synthetic application can be seen from the gram-scale synthesis experiment. The underlying catalytic mechanism involving 'co-adsorption-co-activation' of the coupling partners to form radical species was discerned by combined catalytic measurements, synchrotron X-ray powder diffraction (SXRD)-Rietveld refinement, probe-assisted electron paramagnetic resonance (EPR) spectroscopy, and density functional theory (DFT) calculations.

RESULTS AND DISCUSSION

SYNTHESIS AND CHARACTERISATION

The dual-atom catalysts were synthesized over a specifically chosen hierarchical USY zeolite (SiO_2:Al_2O_3 = 12) by a modular assembly approach by utilizing the underlying principles of coordination (*via* formation of acid-base adducts) chemistry and solid-state (*via* steric confinement) chemistry, as illustrated in the supporting information (see **Figure S1** in the Supporting Information (SI)). The hierarchical property was studied by N_2 adsorption-desorption isotherm, as is presented in **Figure S2** and **Table S1**. A hysteresis loop at the relative pressures P/P_0 of 0.4–1.0 was observed, which is characteristic of a type IV isotherm.[29] This thus indicates a bimodal micro- and mesoporous distribution, with an average diameter of *ca.* 0.72 nm and 15.8 nm, respectively. In a molecular manner, di-basic 2-methylimidazolate ('meIm') was used as a linker to connect multiple cationic metal M^{2+} (M = Co, Ni, Cu, and Zn) nuclei in the micropore of USY. The samples are denoted as Cu_x-Y (where x = 1, 2, and 3), and Cu-M-Y for simplicity. The elemental analysis based on X-ray fluorescence (XRF) spectroscopy shows an increasing trend in the corresponding metal contents upon the application of meIm (**Figure 1a** and **Table S2**). For instance, the Cu:Zn molar ratio is 0.87:1 in Cu-Zn-Y, and the Cu content in Cu_1-Y and Cu_2-Y increases from 2.92 wt% to 5.27 wt% (nearly doubled). In contrast, no change in the metal content was noted without applying 2-meIm from our control experiments, which signifies the successful modular addition of metals within the zeolites. Related Zn-based dual-atoms over a series of ZSM-5 zeolites have been also prepared successfully.[30-31]

'Solid-state' mass spectrometry by matrix-assisted laser desorption/ionization time-of-flight/time-of-flight mass spectrometry (MALDI-TOF/TOF-MS) can be used to probe the metal constituents of the dual-atoms, as the isotope distribution based on natural abundance can reflect the metal nuclearity and elemental composition.[32-33] By carefully tuning the laser power, related bi- and trinuclear extra-framework metal clusters supported on zeolites can be detected, as shown in our recent studies.[30-31] **Figure 1c** shows the mass spectra of Cu_2-Y and Cu-Co-Y (which are the more representative samples as later discussed). Predominant features with the mass intensity ratio of M:M+2:M+4 ~ 100:90:20 (*e.g.*, at m/z of 252:254:256) and M:M+2 ~ 100:50 (*e.g.*, at m/z of 319:321) and in Cu_2-Y and Cu-Co-Y, which suggests the notable presence of

dual-atom 'Cu-Co' and 'Cu_2', respectively. These ratios match with the theoretical mass intensity of dimeric Cu_2 and Cu-Co species based on isotope extrapolation

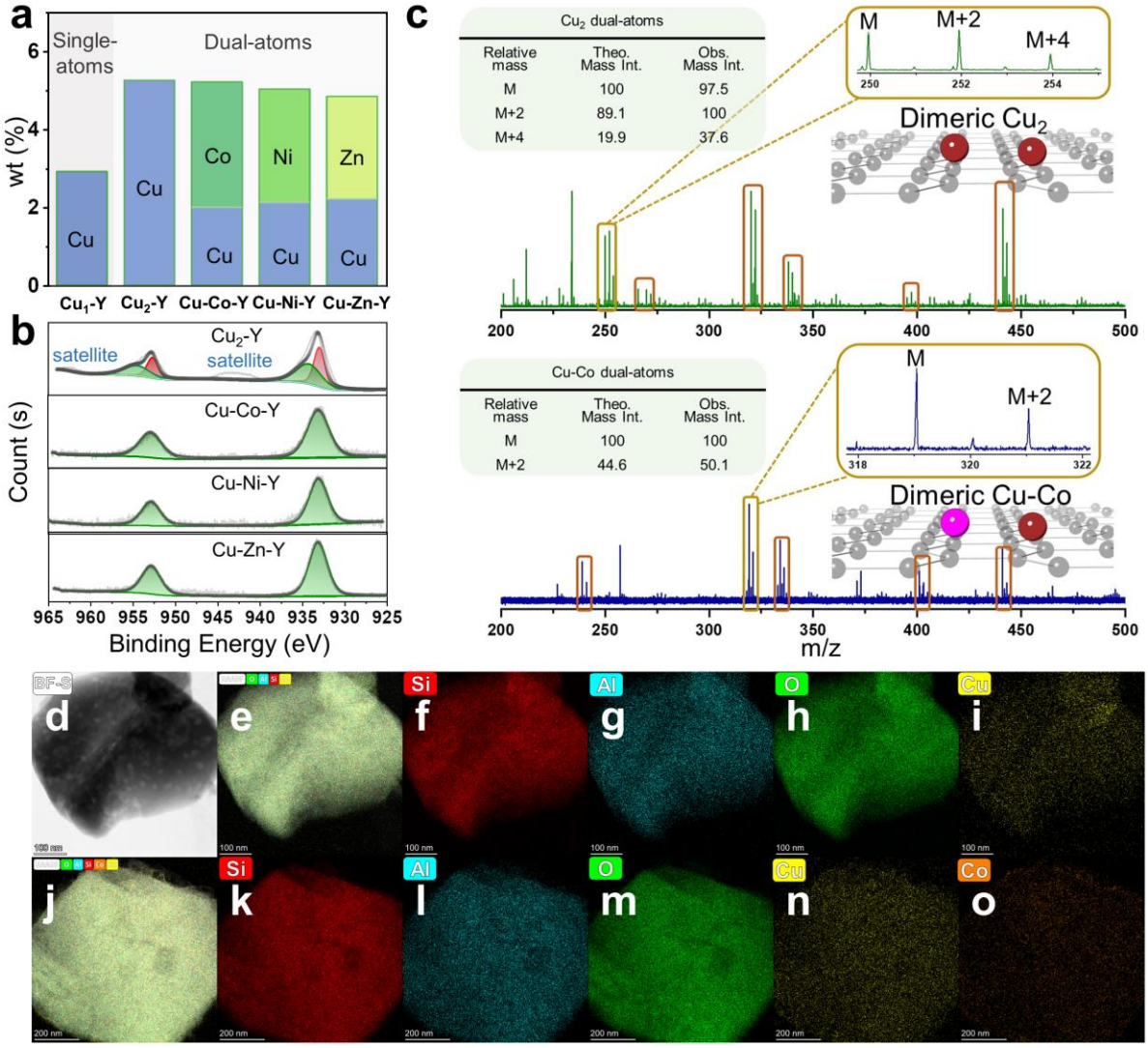

Figure 1. Elemental and morphological characterizations. (**a**) Elemental analysis of Cu_1-Y, Cu_2-Y, Cu-Co-Y, Cu-Ni-Y and Cu-Co-Y, (**b**) Cu 2*p* XPS spectra of Cu_1-Y, Cu_2-Y, and Cu-Co-Y, (**c**) MALDI-TOF/TOF mass spectra of Cu_2-Y and Cu-Co-Y, and TEM-EDX mapping analysis of (**d–i**) Cu_2-Y and (**j–o**) Cu-Co-Y.

(**Scheme S1**). At the lower mass range, the occurrence of 'single-atom' Cu has also been noted, due to potential fragmentation and experimental residual of Cu_1.

Figure S3 shows the SXRD patterns of the metal-modified samples. The space group remains unchanged at ***Fm-3m*** with only marginal shifts of the Bragg peaks, suggesting that the metalation process does not affect the crystalline framework of the host hierarchical USY. No major structural change or metal/metal oxide aggregation has been observed. Highly symmetric Bragg peaks signify the uniform dispersion of the extra-framework species (**Table S3**). As shown in the morphology and transmission electron microscopy energy dispersive X-ray (TEM-EDX) mapping analysis (**Figures 1d–1o**, and **S4**), homogeneous metal distribution and an absence of metal/metal oxides aggregation on the crystal surface were noted.

The electronic properties were probed by combined ultraviolet-visible (UV-vis) spectroscopy, X-ray photoelectron spectroscopy (XPS), and X-ray absorption near-edge spectroscopy (XANES). **Figure S5** shows the UV-vis spectra of the samples of each assembly step. A hypsochromic-bathochromic shift pattern (between 590 and 750 nm) in the *d-d* transition peak of Cu^{2+} species is observed. This can be attributed to the electronic perturbation of Cu^{2+} species upon the application of meIm.[30-31] The XPS and XANES results (**Figures 1b, S6–S7** and **Tables S4–S5**) show the binding energies of the metal species, which reveal their oxidation state of +2 in all the samples (Cu^{2+}-meIm-M^{2+} dual-atom sites).

CATALYTIC PERFORMANCE EVALUATION

The catalytic formation of C–N bonds *via* the CDC mechanism, using a benchmark reaction between 4-methoxyphenol (**1a**) with phenothiazine (**2a**), was performed in a batch reactor with the USY-based catalysts (**Table 1**). The effect of the nuclearity of metal sites was first evaluated (entries 1–4); only a single product (**3a**), from the CDC reaction was detected as confirmed by nuclear magnetic resonance spectroscopy and high-resolution mass spectroscopy. The catalytic reactivity increases over Cu_2-Y catalyst, from nil reactivity over H-USY, to extremely low reactivity over Cu_1-Y, to a turnover frequency (TOF) of 0.251 site^{-1} h^{-1} over Cu_2-Y. The marginal difference in the isolated yields over Cu_2-Y and Cu_3-Y implies that the third metal site does not actively contribute to the reaction process. By varying the elemental composition (entries 3, 5–7), the reactivities over Cu-Co-Y (TOF = 0.322 site^{-1} h^{-1}) are much higher than those over analogous Cu_2-Y (0.251 site^{-1} h^{-1}), Cu-Ni-Y (0.086 site^{-1} h^{-1}), and Cu-Zn-Y (0.097 site^{-1} h^{-1}). The absence of Cu cannot catalyze the amination reaction, as seen in our control experiments (entries 1, 8–9). This high yield from CDC reaction between unprotected phenols and phenothiazines over a heterogeneous catalytic system is remarkable, particularly with an extremely simple and environmentally friendly reaction condition requirement, *i.e.*, room temperature, methanol as solvent, additive-free, and O_2 (and air; entry 10). The reactivity was comparable with various recent findings, such as using the electrocatalytic approach by the Lei group.[34-37]

With the addition of TEMPO (2,2,6,6-tetramethylpiperidine 1-oxyl; radical trap; entry 11), only a trace amount (<1%) of **3a** product was formed, which suggests the involvement of activated radical species (supported by our electron paramagnetic resonance (EPR) spectroscopy study which will be discussed later). This supports previous findings over homogeneous catalysts, where the cross-coupling reaction between **1a** and **2a** involves the dual-radical mechanism (**Scheme S2**).[34, 38] Under this mechanism, both coupling partners are oxidized by the redox-active metal centers to form the corresponding radical species *via* a single-electron transfer (SET) mechanism. We have also considered the potential impact of the residual zeolitic BASs (if present). In the absence of BASs (entry 14, H^+ replaced with Na^+), Cu-Co-Y (Na^+) delivers a marginally affected catalytic activity where the isolated yield of **3a** only dropped slightly from 83% to 73%. It is in stark contrast to various recent studies where such poisoning of BASs has fully impeded the catalytic reactivities.[31, 39] It indicates the minor role of the BASs (if present) in the CDC reaction.

Table 1. Screening of catalysts and conditions. Unless otherwise specified, all reactions were performed with 1a (0.25 mmol), 2a (0.25 mmol), catalyst (100 mg), CH_3OH (3.0 mL), and charged with an O_2 balloon at room temperature for 20 h.

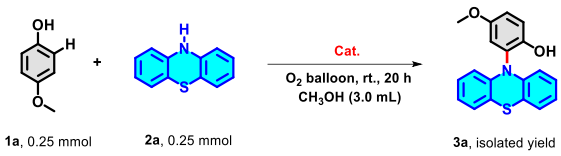

Entry	Catalyst	Isolated yield of 3a (%)	Turnover frequency (site^{-1} h^{-1})
1	H-USY	n.d.	-
2	Cu_1-Y	trace	-
3	Cu_2-Y	83	0.251
4	Cu_3-Y	76	0.136
5	Cu-Co-Y	81	0.322
6	Cu-Ni-Y	23	0.086
7	Cu-Zn-Y	27	0.097
8	Co_1-Y	n.d.	-
9	Co_2-Y	n.d.	-
10	Cu_2-Y with air	45	0.136
11	Cu_2-Y with TEMPO	trace	-
12	Cu_2-Y (doubled catalyst loading)	80	
13	Cu_2-Y (halved catalyst loading)	54	
14	Cu-Co-Y (Na^+ poisoned)	73	

As presented in **Scheme S3**, we have also successfully achieved a direct scale-up of the process, where more than 0.5 g of **3a** product has been yielded with similar catalytic efficiency over Cu-Co-Y. Excellent catalytic recyclability has been achieved (**Figure S8**), with the catalytic reactivity remaining over five cycles. The crystallinity of the samples remained unaltered from our postmortem powder XRD (**Figure S9**) and TEM-EDX mapping analyses (**Figure S10**). Nil metal ion (< 0.3 ppm) was detected from hot filtration experiments.

We subsequently evaluated the reaction kinetics of the CDC reaction over the Cu-M-Y catalysts, with the kinetic data presented in **Figure S11**. The reactions over Cu-Ni-Y, Cu_2-Y, and Cu-Zn-Y were determined as first-order reactions, with the corresponding rate constant k of 0.18, 0.85, and 0.17 g cat^{-1} h^{-1}, respectively. In contrast, the reaction over Cu-Co-Y was determined as a zeroth-order reaction, at k = 0.10 mmol g cat^{-1} h^{-1}.

It is extremely interesting to note such a difference in the TOF and reaction order over these related Cu-M-Y catalysts. In particular, the zeroth-order reaction of Cu-Co-Y suggests that the catalytic reaction is under a diffusion control regime, which hints at a more favored activation of the reaction substrates when compared to other Cu-M-Y analogs. Further mechanistic discussion will be made in the following sections.

To explore the universality of this catalytic scheme, the reaction scope was further extended to structurally different phenol (–H, –Me, –OMe, –OPh, and –OBn) and phenothiazine (–CF_3, –Cl, and –CN) functional groups. A series of phenols **1** and phenothiazines **2** were examined. As

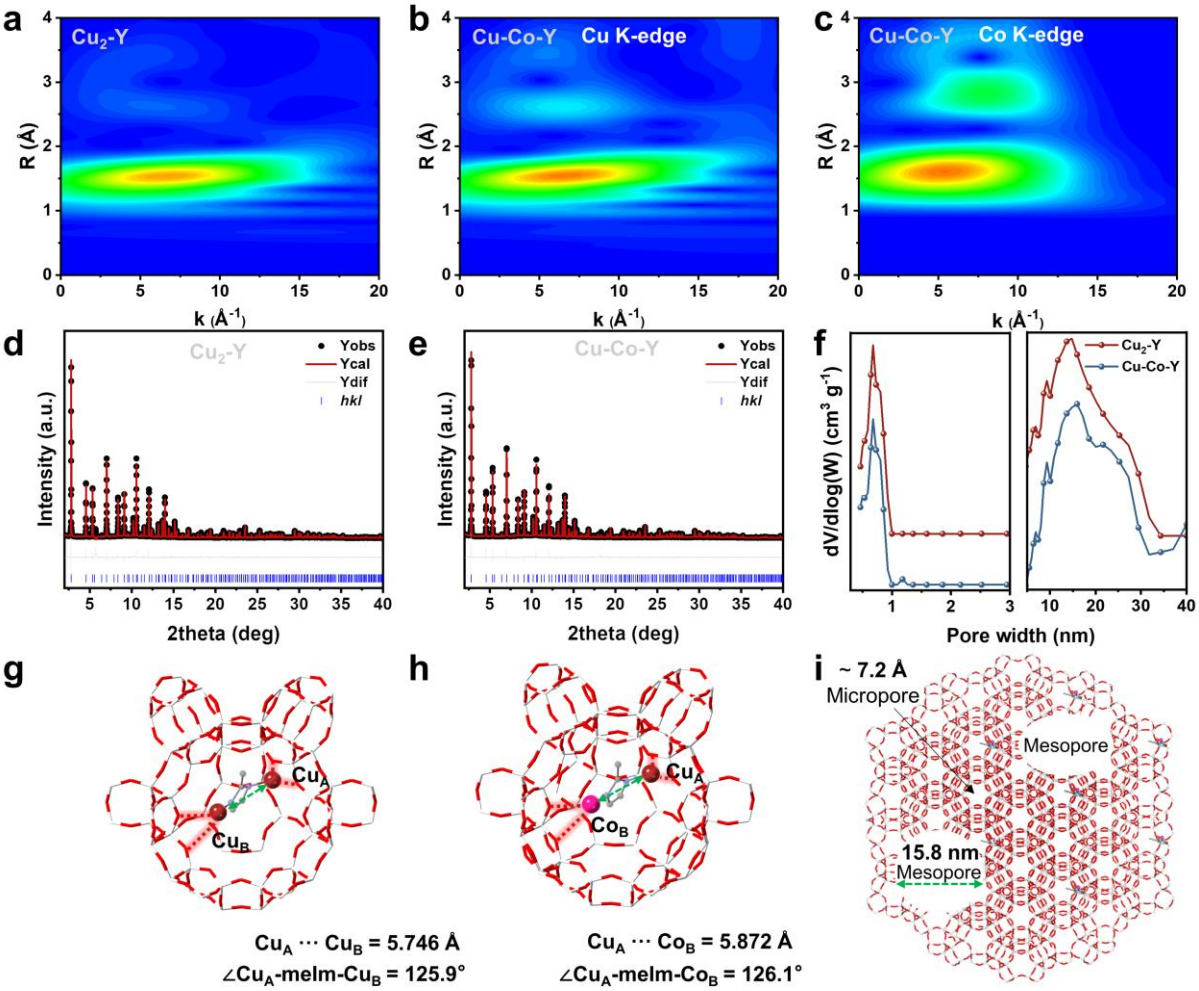

Figure 2. Atomic and structural elucidation of the catalysts. Wavelet transforms for k^3 weighted Cu K-edge EXAFS signal of (**a**) Cu_2-Y and (**b**) Cu-Co-Y, wavelet transform for k^3 weighted Co K-edge EXAFS signal of (**c**) Cu-Co-Y. The Rietveld refinement profiles of high-resolution SXRD of (**d**) Cu_2-Y and (**e**) Cu-Co-Y. (**f**) Pore size distribution profiles of Cu_2-Y and Cu-Co-Y (from microporosity analysis), (**g–h**) the corresponding Rietveld refined crystal structures. (**i**) Schematic illustration of Cu-Co dual-atoms supported on bi-modal meso-micro hierarchical USY zeolite The ligation water molecules and the mirror symmetry of the extra-framework species are disregarded for clarity. Atoms are represented in balls/sticks (dark red = copper, pink = cobalt, grey = carbon, light blue = nitrogen, white = silicon, and red = oxygen).

shown in **Scheme S4**, most of the substrates **2a–2e**, and **2g–2j** underwent amination and delivered the desired products **3a–3e**, and **3g–3j** at moderate to excellent yields. We also noted tolerance in oxazine (**3k**). In addition, we detected nil **3f** product, which suggests the limitation of large estrone molecule (**2f**) in assessing most of the active sites located within the micropores statistically. On the other hand, nil reactivity was noted using diphenylamine as the coupling partner, which can be attributed to the superior stabilization of the *N*-radical intermediates by thiazine/oxazine.

ATOMIC STRUCTURE ELUCIDATION

The catalytic results revealed that the reactivity is highly dependent on the metal nuclearity and constituent composition. We will use Cu_2-Y and Cu-Co-Y for our major illustration, which are the more representative samples. To understand the structure-reactivity correlations, the geometric and electronic structures of the catalytic sites should be further elucidated. The geometry and coordination environments of the metal species were first revealed by EXAFS. Wavelet transformations (WT) were employed (**Figure 2a–c**) to better correlate the k-space (reciprocal) and R-space (real) information. The highest intensity belongs to the lobe centered at k = 4 $Å^{-1}$, R = 1.5 Å, which corresponds to the N or O atoms around the Cu or Co center.

Note that metal–O and metal–N interactions are barely distinguishable by typical non-resonant X-ray techniques because of the proximity of their scattering factors. Long-range Cu–Cu (or Co) scattering path is not observed at

higher radial distances (at k > 10 Å^{-1}, R > 1.5 Å), indicating the absence of metal aggregation. Quantitative profile fitting analyses of the k-space and R-space were conducted to study the scattering paths of Cu/Co–N/O in Cu_2-Y and Cu-Co-Y (see the detailed analyses in **Figures S12–S15** and **Table S6**). The Cu–N/O bond lengths were

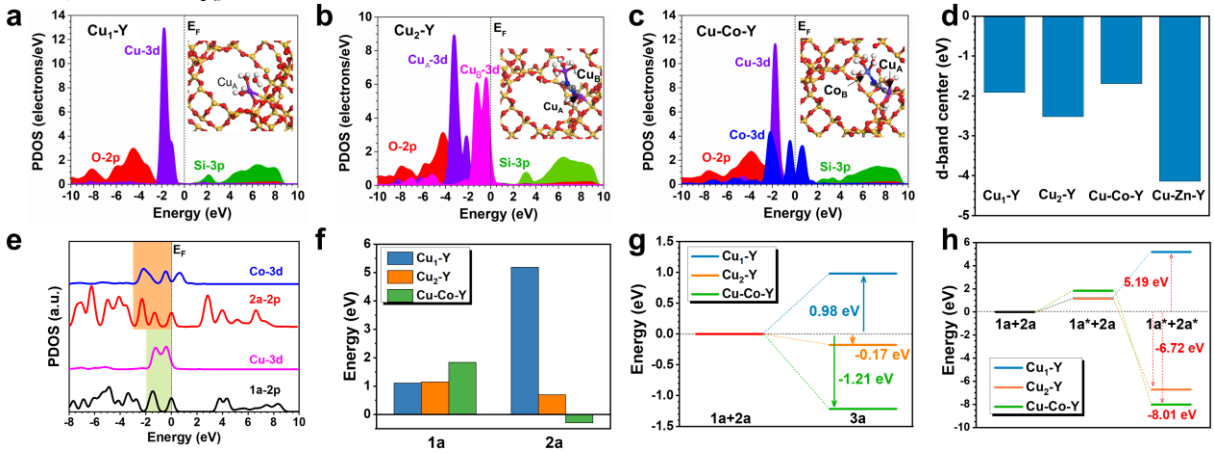

Figure 3. DFT calculations on the adsorption and reaction energetics. The PDOS of (**a**) Cu_1-Y, (**b**) Cu_2-Y, and (**c**) Cu-Co-Y; the inset shows the corresponding optimized structures. Atoms are represented in balls/sticks (purple = Cu, light blue = Co, yellow = Si, red = O, blue = N, grey = C, and white = O). (**d**) Comparison of the d-band centers of Cu_1-Y, Cu_2-Y, Cu-Co-Y and Cu-Zn-Y. (**e**) PDOS comparison of **1a**, **2a**, and the metal sites. (**f**) The adsorption energy barrier of **1a** and **2a**, (**g**) the corresponding reaction energies in the CDC reaction. (**h**) The energy costs for the co-adsorption of reactants in Cu_1-Y, Cu_2-Y, and Cu-Co-Y.

determined as around 2.0 Å with an average Cu–N/O coordination number of about 4 in both samples, where the Co–N/O bond distance was calculated as 2.10 Å with an average coordination number of 4.3.

The Rietveld refinement of SXRD data was then used to discern the atomic parameters of the metal sites within the micropores of USY. The intensities of the Bragg peaks were significantly altered upon the incorporation of the metal species. We have accordingly combined Rietveld refinement of the SXRD and quantitative analysis of EXAFS to elucidate the crystal structures (**Figures 2d**, **2e**, **2g**, **2h**, and **S16–S17**, as done in related studies[39-42]), with the overall site occupancy factors of the metal sites constrained based on our elemental analysis (**Table S2**). The crystallographic locations of the metal nuclei were first identified by the charge-flipping algorithm. We have subsequently employed a stepwise refinement for Cu_x-Z and Cu-M-Y, that is, following along Cu_1-Y, Cu_1-meIm-Y, and finally Cu-M-Y, to refine the corresponding crystallographic metal locations. We noted that two crystallographic metal sites are located around 5.8 Å apart in the micropores of Cu_2-Y and Cu-Co-Y. This atomic separation suggests the presence of a bridging meIm between the two metal nuclei. **Figure 2g–h** displays their optimized crystal structures. The Cu_A site is located close to the zeolite framework near the sodalite cage, while Cu_B/Co_B is located on the opposite side of the supercage. The interatomic angle of ∠Cu_A-meIm-Cu_B is determined as around 145°, which matches the typical values of related zeolitic imidazolate frameworks.[43] Similar atomic structures of Cu-Ni-Y and Cu-Zn-Y have also been observed (**Figure S17**). The corresponding atomic and crystallographic parameters are summarized in **Tables S7–S16**. Taking the unique structural property of the hierarchical USY into account, these dual-atoms are primarily located in the micropores of USY, but larger dimension access is also given to reaction substrates at the micro-mesopores junctions (as presented in the schematic in **Figure 2i**). This can be verified by that nil product has been collected from the coupling between **1a** and large estrone molecule (**2f**), but smaller substrates (**2**) were converted effectively. It can be attributed to the active sites being mainly located at the micropores, instead of the mesopores, based on our porosity analysis (**Table S1**). Hence, the Cu-M dual-atoms supported on this hierarchical USY zeolite, with the dual-atoms predominantly immobilized in the micropores, would not only offer substrate activation within a reasonable molecular separation but also provides a quasi-isolated domain within the mesopore for effective coupling reaction between the activated substrates to proceed, as well as enhanced intracrystalline (meso/micropore) diffusion of substrates and products.

Given that Cu-Co-Y renders a more superior reactivity when compared with Cu_1-Y and its Cu-M-Y analogs, we have accordingly employed DFT calculations to investigate the adsorption preferences, reaction barriers, and activation capability. The projected density of states (PDOS) was first compared, which reveals the electronic structures of the supported dual-atom catalysts (**Figure 3a–c**). For Cu_1-Y, the Cu-3*d* orbitals exhibit a sharp peak at E_v–1.78 eV (E_v = 0 eV) in the PDOS, which acts as the sole site for electron transfer. The O-2*p* orbitals are located below the Cu-3*d* orbitals, whereas the Si-3*p* orbitals dominate the conduction band. For Cu_2-Y, there are two sets of electronic contributions related to Cu. Cu_A is

stabilized by two water molecules with the Cu_A-3*d* orbital at E_v–3.24 eV. In comparison, Cu_B is tightly bound by three water molecules with the Cu_B-3*d* orbitals located near the Fermi level. The O-2*p* orbitals show partial overlap with the Cu_A center while Si-3*p* remains as the conduction band (akin to that in Cu_1-Y). Comparable finding on the electronic structure of Cu_2-Y has also been observed in our XPS measurement with two different binding energies of Cu-2*p* (**Figure S6**), which can be attributed to the distinct chemical nature of the N moieties of the meIm linker (pyridine-like and pyrrole-like, respectively).[44]

Similar binding with water ligands has been noticed in Cu-Co-Y. The Cu center shows an electronic structure comparable to that of Cu_1-Y with the dominant peak at E_v–1.73 eV, whereas the Co-3*d* orbitals demonstrate several peaks covering from E_v to E_v–2.15 eV. The distinct electronic structures of Cu_2-Y and Cu-Co-Y suggest the presence of two different adsorption sites, which warrants an efficient electron transfer for substrate co-adsorption and subsequent co-activation on the dual-atom sites. Also, the improved overlapping between Cu-3*d* and Co-3*d* should offer higher reaction efficiency between the coupling partners. We further compared the *d*-band center of different catalysts, as shown in **Figure 3d**. Compared to Cu_1-Y, although the *d*-band center is lower in Cu_2-Y, the presence of two distinct but neighboring adsorption sites in Cu_2-Y is the key factor that leads to promoted catalytic reactivity due to stable initial binding (co-adsorption) with **1a** and **2a** substrates. A higher *d*-band center is observed in Cu-Co-Y, which could explain why a higher reactivity has been experimentally noted. We have also compared the *d*-band center of Cu-Zn-Y, which is much lower at around –4.2 eV and renders lower catalytic reactivity. As shown in **Figure 3e**, the PDOS study reveals a strong *p*-*d* orbital overlap between the adsorbed substrates and the metal sites. The 2*p* orbitals of **1a** and **2a** match well with the Cu-3*d* and Co-3*d* orbitals, respectively, leading to the strong adsorption of the reactants. Whereas the adsorption energy barrier (mainly from steric hindrance) of **1a** is comparable on Cu_1-Y, Cu_2-Y, and Cu-Co-Y, the adsorption of **2a** on Cu_1-Y and Cu_2-Y has a large energy barrier (**Figure 3f**). This supports the poorer catalytic performance of Cu_1-Y and Cu_2-Y in the cross-coupling reaction compared with that of Cu-Co-Y. In particular, the adsorption of **2a** on Cu-Co-Y is favored by a low energy barrier, which leads to promoted catalytic reactivity. The overall reaction energies have also been compared to indicate the reaction trend (**Figure 3g**). Cu-Co-Y shows a much more favorable trend for the formation of **3a** with the overall reaction energies of –1.21 eV (*cf.* –0.17 eV for Cu_2-Y), respectively, which agrees with our kinetic data (**Figure S11**). A significant energy barrier of 0.98 eV in Cu_1-Y suppresses the cross-coupling reaction. Since the co-adsorption of **1a** and **2a** is critical to the subsequent cross-coupling reaction pathway, the overall energy cost (resultant of adsorption and reaction energies) is also an important consideration, as shown in **Figure 3h**. Due to the unfavorable adsorption of **2a** on Cu_1-Y, the formation of **3a** is greatly hindered. Stable bindings of **1a** and **2a** on Cu-Co-Y, on the other hand, warrant higher catalytic reactivity as observed experimentally.

One reason we observed this subtle rate-enhanced amination reaction is because of the excellent energy matching between the coupling partners and the two neighboring metal species in the dual-atom active sites. The favored adsorptions of **1a** and **2a** on Cu-Co dual-atoms have been calculated above as the key factor in promoting the reactivity. Probe-assisted EPR experiments were further employed to elucidate the structure-reactivity correlations by studying the coordination geometries and the adsorption preferences of the reaction substrates of Cu and Co sites.

Adsorption binding of reaction substrates with EPR active centers can significantly affect the peak intensity by altering the overall unpaired electrons in the system.[45-46] The continuous-wave EPR spectra of Cu_1-Y, Cu_2-Y and Cu-Co-Y before and after loading of individual substrates (**1a** and **2a**) were measured. The probe-assisted EPR spectra of Cu_1-Y, Cu_2-Y, and Cu-Co-Y are presented in **Figures 4** and **S18**. No noticeable change of the *g*-tensors and signal intensities has been observed in the EPR spectra of Cu_1-Y upon the adsorption of **1a** or **2a** (**Figure S18** and **Tables S17–S18**), which supports the minimal interactions between Cu sites and substrates (**1a** and **2a**) as computed by our DFT calculation. On the contrary, the EPR signal of Cu_2-Y is significantly broader than that of Cu_1-Y due to stronger dipolar exchange interactions between nearby Cu sites in Cu_2 (Cu_A···Cu_B = 5.746 Å). Slight hyperfine features appeared in the low-field part of the spectrum ($g_{//}$ = 2.42, $A_{//}$ = 480 MHz).[47] We observed altered *g*- and *A*-tensors of Cu^{2+} and a noticeable decrease in signal intensity upon the adsorption of **1a** or **2a** on Cu_2-Y (**Figure 4a–b** and **Tables S17** and **S19**). In the case of Cu_2-Y+**2a**, a new intense high-field narrow band with g = 2.003 without any hyperfine structure, which can be attributed to the formation of **2a** radical by Cu^{2+} reduction (giving EPR silent Cu^{+}) through electron transfer between Cu^{2+} and **2a**.[48-50] Likewise, the EPR signals of Cu^{2+} in Cu-Co-Y decreased notably upon **1a** and **2a** adsorption, and the *g*- and *A*-tensors were altered (**Figure 4c–d** and **Tables S17** and **S20**). The absence of a signal attribution of Co^{2+} (d^7, S = 3/2, high spin) is potentially due to the fast relaxation and only becomes detectable at < 10 K.[51-52] The calibrated EPR intensity of the newly formed radical is apparently 8.2 times larger in Cu-Co-Y than Cu_2-Y, which infers more efficient electron transfer between Cu-Co-Y and **2a** compared with Cu_2-Y (**Figure S19** and **Table S21**).

The adsorption configurations of **1a** and **2a**, in terms of atomic distances, over Cu-Co-Y, have been further revealed by combined probe-assisted SXRD and DFT calculations (**Figures 4e–h**, **S20**, and **Tables S22–S26**).[42, 53] Asymmetric binding preferences are noted in Cu-Co-Y+**1a** and Cu-Co-Y+**2a**, with O_{1a}···Cu_A = 1.846(2) Å, O_{1a}···Co_B =

5.580(3) Å, N_{2a}···Co_B = 3.456(2), and N_{2a}···Cu_A = 4.283(2) Å, suggesting that more favored adsorption preferences between the Cu···**1a** pair, as well as the Co···**2a** pair. As a result, we propose a reaction mechanism for this CDC reaction based on a 'co-adsorption-co-activation' model for dual-atom Cu-Co-Y (**Figure 4i**). The synergy between Cu and Co in Cu-Co-Y can greatly promote the adsorption and electron transformation of **2a**, which is in great agreement with our catalytic and DFT findings. This also explains that

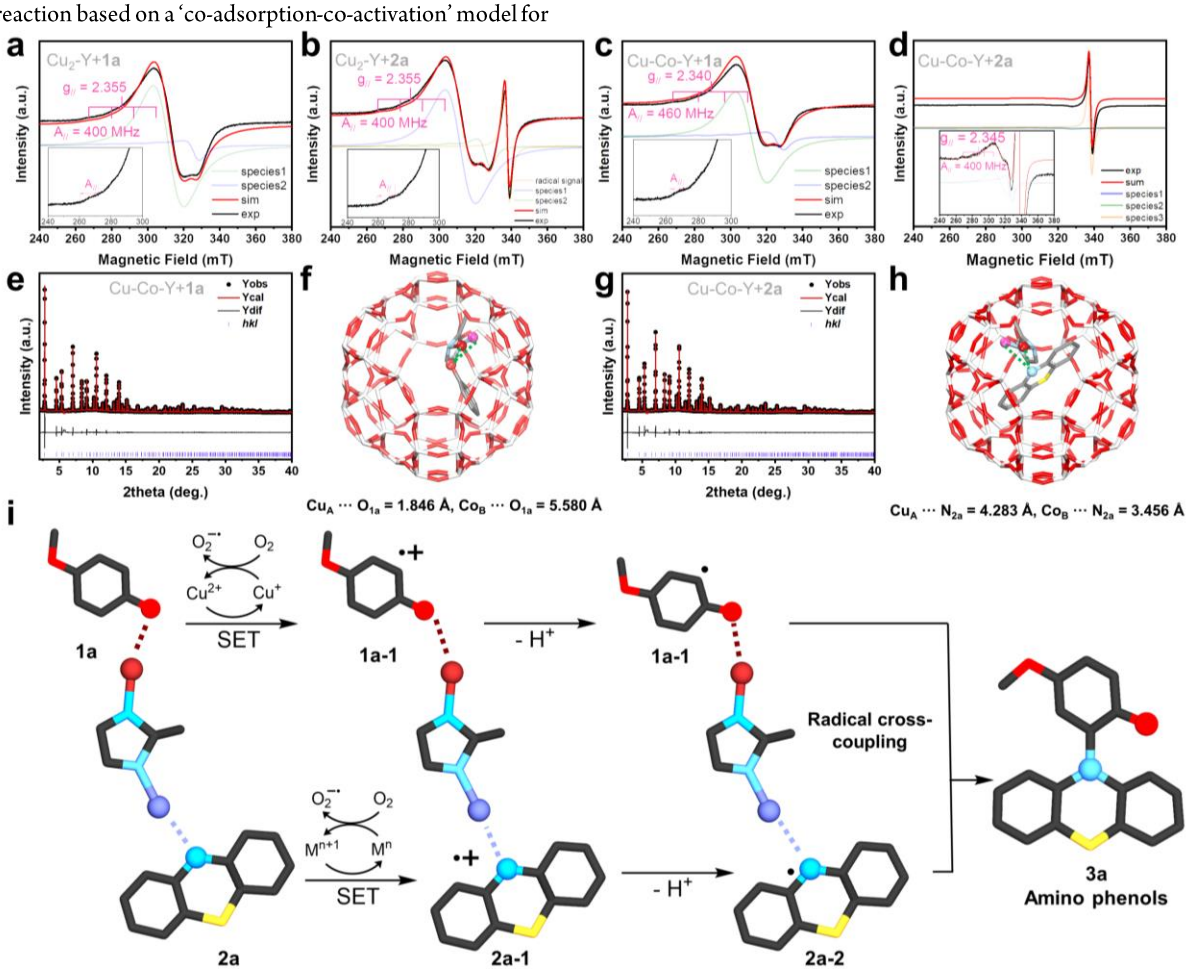

Figure 4. Adsorption configuration investigation. Probe-assisted EPR spectra measured at 77 K of (**a, b**) Cu_2-Y+**1a**, and Cu_2-Y+**2a**, and (**c, d**) Cu-Co-Y+**1a,** and Cu-Co-Y+**2a**. The Rietveld refinements of SXRD patterns, and the derived crystal structure, further optimized by DFT calculations, of Cu-Co-Y pre-adsorbed with (**e, f**) **1a** and (**g, h**) **2a**. (**i**) Proposed reaction mechanism of the radical cross-coupling between **1a** and **2a.**

the analogous Cu-Ni-Y and Cu-Zn-Y samples show much inferior catalytic reactivity as Co^{2+} (d^7) and Cu^{2+} (d^9) are well-known radical initiators.

CONCLUSIONS

To conclude, we have presented the construction of Cu-based dual-atom catalysts supported on hierarchical USY zeolites for the CDC reaction between unprotected phenols and phenothiazines. The superior reactivity, at highly simple and environmentally friendly reaction conditions, has been attributed to the precise synthesis of the active sites within the micropores, and the facile intracrytalline diffusion of heterocyclic organic substrates along the mesopores.

The detailed atomic and structural parameters of these dual-atom catalysts have been determined by our multi-modal characterization. While the metal sites in the dual-atoms are located about 5.8 Å apart, they can synergistically offer separate active sites for substrate co-adsorption in proximity. The supported Cu-Co dual-atoms uniquely exhibit superior performance in the production of aminated phenols in the absence of any additives. The reactivity is pleasingly comparable with the *state-of-the-art* homogeneous and electrocatalytic systems operating under more forceful conditions. A rational structure-reactivity interplay between hierarchical zeolite architecture, reaction energetics, and catalytic properties has been discerned. The intricate bimodal micro- and mesoporous distribution within the hierarchical zeolites not only offers rigid support for the homogeneous immobilization of metal species but also provides a quasi-isolated cavity for effective radical coupling. This will bring a realizable leap toward the next-generation heterogeneous catalysts at the molecular homogeneous dimension for the sustainable production of fine chemicals.

ASSOCIATED CONTENT

Supporting Information. This material is available free of charge via the Internet at http://pubs.acs.org.
Additional experimental details, materials, methods, and supplementary characterization results, including, SXRD, Raman, EPR, microscopic images, EXAFS fittings, catalytic results, elemental analysis, and surface porosity analysis.

AUTHOR INFORMATION

Corresponding Author

* bhuang@polyu.edu.hk (B. Huang), taoyuanliang@gxu.edu.cn (T. Liang), benedict.tw.lo@polyu.edu.hk (T. W. B. Lo)

Author Contributions

§: T.C. and Y.W. contributed equally to this work.

Funding Sources

TWBL thank the National Natural Science Foundation of China (22172136), the Hong Kong Research Grants Council (15301521, 15300819, and 15305722), the Department of Science and Technology of Guangdong Province (2021A1515010218), PolyU start-up SHS fund (BDC3), for financial support. TL thank the National Natural Science Foundation of China (22201048) and the Natural Science Foundation of Guangxi Province (2022GXNSFBA035480) for financial support.

ACKNOWLEDGMENT

We thank SPring-8 (2021B1100 and 2021B0099) for beamtimes; UMF, UCEA, ULS of HKPU for the support in material characterization.

REFERENCES

(1) Chen, Y.; Ji, S.; Sun, W.; Chen, W.; Dong, J.; Wen, J.; Zhang, J.; Li, Z.; Zheng, L.; Chen, C.; Peng, Q.; Wang, D.; Li, Y., Discovering Partially Charged Single-Atom Pt for Enhanced Anti-Markovnikov Alkene Hydrosilylation. *J. Am. Chem. Soc.* **2018,** *140* (24), 7407-7410.

(2) Zhang, J.; Wang, Z. Y.; Chen, W. X.; Xiong, Y.; Cheong, W. C.; Zheng, L. R.; Yan, W. S.; Gu, L.; Chen, C.; Peng, Q.; Hu, P.; Wang, D. S.; Li, Y. D., Tuning Polarity of Cu-O Bond in Heterogeneous Cu Catalyst to Promote Additive-free Hydroboration of Alkynes. *Chem* **2020,** *6* (3), 725-737.

(3) Ji, G.; Zhao, L.; Wei, J.; Cai, J.; He, C.; Du, Z.; Cai, W.; Duan, C., A Metal-Organic Framework as a Multiphoton Excitation Regulator for the Activation of Inert C(sp(3))-H Bonds and Oxygen. *Angew. Chem. Int. Ed.* **2022,** *61* (2), e202114490.

(4) Djakovitch, L.; Felpin, F.-X., Direct C sp2–H and C sp3–H Arylation Enabled by Heterogeneous Palladium Catalysts. *ChemCatChem* **2014,** *6*, 2175-2187.

(5) Punzi, A.; Zappimbulso, N.; Farinola, G. M., Direct Arylations via C-H Bond Functionalization of 1,2,3-Triazoles by a Reusable Pd/C Catalyst Under Solvent-Free Conditions. *Eur. J. Org. Chem.* **2020,** *2020*, 3229-3234.

(6) Bhattacharjee, P.; Boruah, P. K.; Das, M. R.; Bora, U., Direct C–H bond activation: palladium-on-carbon as a reusable heterogeneous catalyst for C-2 arylation of indoles with arylboronic acids. *New J. Chem.* **2020,** *44*, 7675-7682.

(7) Vercammen, J.; Bocus, M.; Neale, S.; Bugaev, A.; Tomkins, P.; Hajek, J.; Van Minnebruggen, S.; Soldatov, A.; Krajnc, A.; Mali, G.; Van Speybroeck, V.; E. De Vos, D., Shape-selective C–H activation of aromatics to biarylic compounds using molecular palladium in zeolites. *Nat. Catal.* **2020,** *3*, 1002-1009.

(8) Tran, T. V.; Le, H. T. N.; Ha, H. Q.; Duong, X. N. T.; Nguyen, L. H. T.; Doan, T. L. H.; Nguyen, H. L.; Truong, T., A five coordination Cu(II) cluster-based MOF and its application in the synthesis of pharmaceuticals: Via sp3 C-H/N-H oxidative coupling. *Catal. Sci. Technol.* **2017,** *7*, 3453-3458.

(9) Chen, S. C.; Li, N.; Tian, F.; Chai, N. N.; He, M. Y.; Chen, Q., Mild direct amination of benzoxazoles using interpenetrating Cobalt(II)-based metal-organic framework as an efficient heterogeneous catalyst. *Mol. Catal.* **2018,** *450*, 104-111.

(10) Truong, T.; Nguyen, K. D.; Doan, S. H.; Phan, N. T. S., Efficient and recyclable Cu2(BPDC)2(DABCO)-catalyzed direct amination of activated sp3 C–H bonds by N–H heterocycles. *Appl. Catal., A* **2016,** *510*, 27-33.

(11) Tran, N. T. T.; Tran, Q. H.; Truong, T., Removable bidentate directing group assisted-recyclable metal organic frameworks-catalyzed direct oxidative amination of Sp2 C-H bonds. *J. Catal.* **2014,** *320*, 9-15.

(12) Yuan, Z.; Liu, B.; Zhou, P.; Zhang, Z.; Chi, Q., Preparation of nitrogen-doped carbon supported cobalt catalysts and its application in the reductive amination. *J. Catal.* **2019,** *370*, 347-356.

(13) Singh, H.; Pal, P.; Sen, C.; Panda, A. B.; Ghosh, S. C., Heterogeneous Cu-MnO-Catalyzed Direct C–H Amination of Azoles Using O2 as the Sole Oxidant. *Asian J. Org. Chem.* **2017,** *6*, 702-706.

(14) Tang, D. T. D.; Collins, K. D.; Glorius, F., Completely regioselective direct C-H functionalization of benzo[b]thiophenes using a simple heterogeneous catalyst. *J. Am. Chem. Soc.* **2013,** *135*, 7450-7453.

(15) Gava, R.; Biffis, A.; Tubaro, C.; Zaccheria, F.; Ravasio, N., Heterogeneous copper-based catalysts for the amidation of activated C–H bonds. *Catal. Commun.* **2013,** *40*, 63-65.

(16) Chen, J.; He, L.; Natte, K.; Neumann, H.; Beller, M.; Wu, X.-F., Palladium@Cerium(IV) Oxide-Catalyzed Oxidative Synthesis of N-(2-Pyridyl)indoles via C–H Activation Reaction. *Adv. Synth. Catal.* **2014,** *356*, 2955-2959.

(17) He, J.; Dhakshinamoorthy, A.; Primo, A.; Garcia, H., Iron Nanoparticles Embedded in Graphitic Carbon Matrix as Heterogeneous Catalysts for the Oxidative C–N Coupling of Aromatic N–H Compounds and Amides. *ChemCatChem* **2017,** *9*, 3003-3012.

(18) Chng, L. L.; Zhang, J.; Yang, J.; Amoura, M.; Ying, J. Y., C-C bond formation via C-H activation and C-N bond formation via oxidative amination catalyzed by palladium-polyoxometalate nanomaterials using dioxygen as the terminal oxidant. *Adv. Synth. Catal.* **2011,** *353*, 2988-2998.

(19) Cui, X.; Li, W.; Ryabchuk, P.; Junge, K.; Beller, M., Bridging homogeneous and heterogeneous catalysis by heterogeneous single-metal-site catalysts. *Nat. Catal.* **2018,** *1*, 385-397.

(20) Liu, L.; Meira, D. M.; Arenal, R.; Concepcion, P.; Puga, A. V.; Corma, A., Determination of the Evolution of Heterogeneous Single Metal Atoms and Nanoclusters under Reaction Conditions: Which Are the Working Catalytic Sites? *ACS Catal.* **2019,** *9* (12), 10626-10639.

(21) Wang, A.; Li, J.; Zhang, T., Heterogeneous single-atom catalysis. *Nat. Rev. Chem.* **2018,** *2*, 65-81.

(22) Valentini, F.; Piermatti, O.; Vaccaro, L., Metal nanoparticles as sustainable tools for C−N bond formation via C−H activation. *Molecules* **2021,** *26,* 4106.

(23) Li, J.; Huang, H.; Xue, W.; Sun, K.; Song, X.; Wu, C.; Nie, L.; Li, Y.; Liu, C.; Pan, Y.; Jiang, H. L.; Mei, D.; Zhong, C., Self-adaptive dual-metal-site pairs in metal-organic frameworks for selective CO2 photoreduction to CH4. *Nat. Catal.* **2021,** *4,* 719-729.

(24) Mitchell, S.; Pérez-Ramírez, J., Atomically precise control in the design of low-nuclearity supported metal catalysts. *Nat. Rev. Mater.* **2021,** *6,* 969-985.

(25) Li, L.; Yuan, K.; Chen, Y., Breaking the Scaling Relationship Limit: From Single-Atom to Dual-Atom Catalysts. *Acc. Mater. Res.* **2021,** *2022,* 584-596.

(26) Huang, L.; Chen, J.; Gan, L.; Wang, J.; Dong, S., Single-atom nanozymes. *Sci. Adv.* **2019,** *5,* eaav5490.

(27) Ye, L.; Song, Q.; Lo, B. T. W.; Zheng, J.; Kong, D.; Murray, C. A.; Tang, C. C.; Tsang, S. C. E., Decarboxylation of Lactones over Zn/ZSM-5: Elucidation of the Structure of the Active Site and Molecular Interactions. *Angew. Chem. Int. Ed.* **2017,** *56,* 10711-10716.

(28) Chen, T.; Ellis, I.; Hooper, T. J. N.; Liberti, E.; Ye, L.; Lo, B. T. W.; O'Leary, C.; Sheader, A. A.; Martinez, G. T.; Jones, L.; Ho, P. L.; Zhao, P.; Cookson, J.; Bishop, P. T.; Chater, P.; Hanna, J. V.; Nellist, P.; Edman Tsang, S. C., Interstitial boron atoms in the palladium lattice of an industrial type of nanocatalyst: Properties and structural modifications. *J. Am. Chem. Soc.* **2019,** *141,* 19616-19624.

(29) Shamzhy, M.; Opanasenko, M.; Concepcion, P.; Martinez, A., New trends in tailoring active sites in zeolite-based catalysts. *Chem. Soc. Rev.* **2019,** *48* (4), 1095-1149.

(30) Chen, T. X.; Wang, Y.; Xue, Q.; Wun, C. K. T.; So, P. K.; Yung, K. F.; Wu, T. S.; Soo, Y. L.; Taniya, K.; Day, S.; Tang, C. C.; Li, Z. H.; Huang, B. L.; Tsang, S. C. E.; Wong, K. Y.; Lo, T. W. B., Article Atomically precise bimetallic metal ensembles with tailorable synergistic effects. *Cell Reports Phys. Sci.* **2022,** 3 (4), 100850.

(31) Wun, C. K. T.; Mok, H. K.; Chen, T.; Wu, T.-S.; Taniya, K.; Nakagawa, K.; Day, S.; Tang, C. C.; Huang, Z.; Su, H.; Yu, W.-Y.; Lee, T. K. W.; Lo, T. W. B., Atomically dispersed 3d metal bimetallic dual-atom catalysts and classification of the structural descriptors. *Chem Cat.* **2022,** *2,* 2346-2363.

(32) Evans, C.; Mackay, K. M.; Nicholson, B. K., The formation of mixed germanium–cobalt carbonyl clusters: an electrospray mass spectrometric study, and the structure of a high-nuclearity [Ge2Co10(CO)24]2− anion. *Dalton Trans.* **2001,** 1645-1649.

(33) Wang, Z.; Su, H. F.; Gong, Y. W.; Qu, Q. P.; Bi, Y. F.; Tung, C. H.; Sun, D.; Zheng, L. S., A hierarchically assembled 88-nuclei silver-thiacalix[4]arene nanocluster. *Nat. Commun.* **2020,** *11* (1), 308.

(34) Tang, S.; Wang, S.; Liu, Y.; Cong, H.; Lei, A., Electrochemical Oxidative C-H Amination of Phenols: Access to Triarylamine Derivatives. *Angew. Chem. Int. Ed.* **2018,** *57* (17), 4737-4741.

(35) Tang, S.; Zeng, L.; Lei, A., Oxidative R1-H/R2-H Cross-Coupling with Hydrogen Evolution. *J. Am. Chem. Soc.* **2018,** *140,* 13128-13135.

(36) Liu, K.; Tang, S.; Wu, T.; Wang, S.; Zou, M.; Cong, H.; Lei, A., Electrooxidative para-selective C-H/N-H cross-coupling with hydrogen evolution to synthesize triarylamine derivatives. *Nat. Commun.* **2019,** *10* (1), 639.

(37) Patureau, F. W.; Patureau, F. W., The Phenol-Phenothiazine Coupling: an Oxidative Click Concept. *ChemCatChem* **2019,** *11,* 5227-5231.

(38) Zhao, Y.; Huang, B.; Yang, C.; Li, B.; Gou, B.; Xia, W., Photocatalytic Cross-Dehydrogenative Amination Reactions between Phenols and Diarylamines. *ACS Catal.* **2017,** *7,* 2446-2451.

(39) Zhao, P.; Ye, L.; Sun, Z.; Lo, B. T. W.; Woodcock, H.; Huang, C.; Tang, C.; Kirkland, A. I.; Mei, D.; Edman Tsang, S. C., Entrapped Single Tungstate Site in Zeolite for Cooperative Catalysis of Olefin Metathesis with Brønsted Acid Site. *J. Am. Chem. Soc.* **2018,** *140,* 6661-6667.

(40) Lo, B. T. W.; Ye, L.; Tsang, S. C. E., The Contribution of Synchrotron X-Ray Powder Diffraction to Modern Zeolite Applications: A Mini-review and Prospects. *Chem* **2018,** *4,* 1-31.

(41) Lin, W.-C.; Wu, S.; Li, G.; Ho, P.-L.; Ye, Y.; Zhao, P.; Day, S.; Tang, C.; Chen, W.; Zheng, A.; Lo, B. T. W.; Edman Tsang, S. C., Cooperative catalytically active sites for methanol activation by single metal ion-doped H-ZSM-5. *Chem. Sci.* **2021,** *12,* 210-219.

(42) Ye, L.; Song, Q.; Lo, B. T. W.; Zheng, J.; Kong, D.; Murray, C. A.; Tang, C. C.; Tsang, S. C. E., Decarboxylation of Lactones over Zn/ZSM-5: Elucidation of the Structure of the Active Site and Molecular Interactions. *Angew. Chem. Int. Ed.* **2017,** *56* (36), 10711-10716.

(43) Zheng, B.; Sant, M.; Demontis, P.; Suffritti, G. B., Force Field for Molecular Dynamics Computations in Flexible ZIF-8 Framework. *J. Phys. Chem. C* **2012,** *116* (1), 933-938.

(44) Richaud, A.; Barba-Behrens, N.; Méndez, F., Chemical reactivity of the imidazole: A semblance of pyridine and pyrrole? *Org. Lett.* **2011,** *13,* 972-975.

(45) Peng, Y. K.; Tsang, S. C. E., Facet-dependent photocatalysis of nanosize semiconductive metal oxides and progress of their characterization. *Nano Today* **2018,** *18,* 15-34.

(46) Xue, Q.; Ng, B. K. Y.; Man, H. W.; Wu, T. S.; Soo, Y. L.; Li, M. M.; Kawaguchi, S.; Wong, K. Y.; Tsang, S. C. E.; Huang, B.; Lo, T. W. B., Controlled synthesis of Bi- And tri-nuclear Cu-oxo nanoclusters on metal-organic frameworks and the structure-reactivity correlations. *Chem. Sci.* **2022,** *13,* 50-58.

(47) Kang, X.; Li, L.; Sheveleva, A.; Han, X.; Li, J.; Liu, L.; Tuna, F.; McInnes, E. J. L.; Han, B.; Yang, S.; Schroder, M., Electro-reduction of carbon dioxide at low over-potential at a metal-organic framework decorated cathode. *Nat. Commun.* **2020,** *11* (1), 5464.

(48) Rupert, J. P., Electron spin resonance spectra of interlamellar copper(II)-arene complexes on montmorillonite. *J. Phys. Chem.* **1973,** *77,* 784-790.

(49) Chon, H.; Seo, G.; Ahn, B. J., Interaction of furans with Cu(II)Y zeolite catalysts. *J. Catal.* **1983,** *80,* 90-96.

(50) Ma, Y.; Han, X.; Xu, S.; Wang, Z.; Li, W.; da Silva, I.; Chansai, S.; Lee, D.; Zou, Y.; Nikiel, M.; Manuel, P.; Sheveleva, A. M.; Tuna, F.; McInnes, E. J. L.; Cheng, Y.; Rudić, S.; Ramirez-Cuesta, A. J.; Haigh, S. J.; Hardacre, C.; Schröder, M.; Yang, S., Atomically Dispersed Copper Sites in a Metal–Organic Framework for Reduction of Nitrogen Dioxide. *J. Am. Chem. Soc.* **2021,** *143,* 10977-10985.

(51) Pietrzyk, P.; Sojka, Z., Co2+/Co0 redox couple revealed by EPR spectroscopy triggers preferential coordination of reactants during SCR of NOx with propene over cobalt-exchanged zeolites. *Chem. Commun.* **2007,** 1930-1932.

(52) Weckhuysen, B. M.; Verberckmoes, A. A.; Uytterhoeven, M. G.; Mabbs, F. E.; Collison, D.; de Boer, E.; Schoonheydt, R. A., Electron Spin Resonance of High-Spin Cobalt in Microporous Crystalline Cobalt-Containing Aluminophosphates. *J. Phys. Chem. B* **2000,** *104,* 37-42.

(53) Van Aelst, J.; Verboekend, D.; Philippaerts, A.; Nuttens, N.; Kurttepeli, M.; Gobechiya, E.; Haouas, M.; Sree, S. P.; Denayer, J. F. M.; Martens, J. A.; Kirschhock, C. E. A.; Taulelle, F.; Bals, S.; Baron, G. V.; Jacobs, P. A.; Sels, B. F., Catalyst Design by NH4OH Treatment of USY Zeolite. *Adv. Funct. Mater.* **2015,** *25*, 7130-7144.

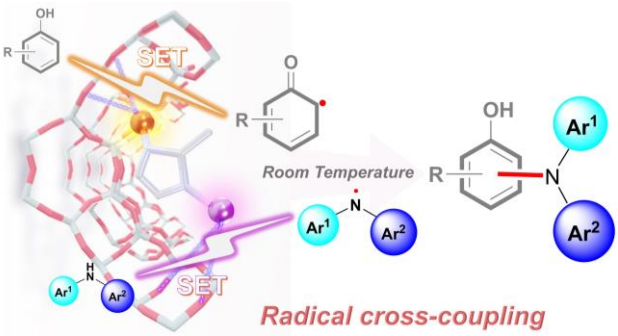
OH
R
SET
O
R
Room Temperature
OH
Ar1
R
N
Ar2
Ar1
N
Ar2
H
N
Ar1
Ar2
SET
Radical cross-coupling